


Determining the refractive index dispersion and thickness of hot-pressed chalcogenide thin films from an improved Swanepoel method

Y. Fang¹  · D. Jayasuriya¹ · D. Furniss¹ · Z. Q. Tang¹ ·
Ł. Sojka^{1,2} · C. Markos^{1,3} · S. Sujecki^{1,2} · A. B. Seddon¹ ·
T. M. Benson¹

Received: 7 March 2017 / Accepted: 16 May 2017 / Published online: 3 June 2017
© The Author(s) 2017. This article is an open access publication

Abstract The well-known method presented by Swanepoel can be used to determine the refractive index dispersion of thin films in the near-infrared region from wavelength values at maxima and minima, only, of the transmission interference fringes. In order to extend this method into the mid-infrared spectral region (our measurements are over the wavelength range from 2 to 25 μm), the method is improved by using a two-term Sellmeier model instead of the Cauchy model as the dispersive equation. Chalcogenide thin films of nominal batch composition $\text{As}_{40}\text{Se}_{60}$ (at.%) and $\text{Ge}_{16}\text{As}_{24}\text{Se}_{15.5}\text{Te}_{44.5}$ (at.%) are prepared by a hot-pressing technique. The refractive index dispersion of the chalcogenide thin films is determined by the improved method with a standard deviation of less than 0.0027. The accuracy of the method is shown to be better than 0.4% at a wavelength of 3.1 μm by comparison with a benchmark refractive index value obtained from prism measurements on $\text{Ge}_{16}\text{As}_{24}\text{Se}_{15.5}\text{Te}_{44.5}$ material taken from the same batch.

Keywords Chalcogenide glasses · Refractive index · Dispersion

1 Introduction

A chalcogenide glass is a glass containing one or more Group 16 elements of the Periodic Table, sulfur (S), selenium (Se), or tellurium (Te), usually formulated with additions of germanium, arsenic or antimony to increase glass stability and robustness (Seddon 1995).

✉ T. M. Benson
Trevor.Benson@nottingham.ac.uk

¹ Mid-Infrared Photonics Group, George Green Institute for Electromagnetics Research, Faculty of Engineering, University of Nottingham, University Park, Nottingham NG7 2RD, UK

² Institute of Telecommunication, Teleinformatics and Acoustics, Wrocław University of Technology, Wybrzeże Wyspińskiego 27, 50-370 Wrocław, Poland

³ DTU Fotonik, Department of Photonics Engineering, Technical University of Denmark, Ørstedes Plads 343, 2800 Kongens Lyngby, Denmark

Since chalcogenide glasses provide a wide range of glass compositions, different physical properties can be achieved, including refractive index. The properties of mid-infrared (MIR) transparency, high refractive index, low phonon energy, high optical non-linearity (Zakery and Elliott 2003), and an ability to doped them with rare-earth element ions (Sanghera and Aggarwal 1999; Sanghera et al. 2009; Tang et al. 2015; Falconi et al. 2016), make chalcogenide glasses attractive for use in planar photonic integrated circuits (Seddon et al. 2006, 2014; Abdel-Moneim et al. 2015), and narrow- and broad-band fibre-based laser sources (Petersen et al. 2014) and amplifiers (Hu et al. 2015; Falconi et al. 2017) for the MIR. Although much research effort has been paid to the development and characterisation of chalcogenide glasses for photonics, relatively little refractive index dispersion data are presently available at MIR wavelengths, see for example: Orava et al. (2009), Qiao et al. (2011), Dantanarayana et al. (2014), Gleason et al. (2016), Wang et al. (2017) and references therein.

Refractive index, and very often its wavelength dispersion, is one of the key parameters that influences the design of optical components. Techniques commonly used for refractive index measurement include the modelling of transmission or reflection spectroscopic data (Swanepoel 1985; Marquez et al. 1998), spectroscopic ellipsometry (Orava et al. 2009; Wang et al. 2017), prism coupling (Carlie et al. 2011), grating coupling (Laniel et al. 2003), and the measurement of the minimum deviation angle of light passing through a prism (Fang et al. 2016). Several of these techniques require intensive sample preparation, are time consuming, and are costly to conduct. More importantly, it has until recently been difficult to apply some of these techniques to the MIR spectral region because of the paucity of suitable beam sources (Carlie et al. 2011). Carlie et al. (2011) modified a commercial system prism coupling system (Metricron model 2010) using additional laser sources, detectors, and a GaP prism in order to enable the measurement of refractive index dispersion at spot wavelengths over the 1.5–10.6 μm range and used it to determine the refractive index of As_2Se_3 bulk glass and thin films across this wavelength region to an accuracy of ± 0.001 . Due to the high accuracy of the method the authors were able to compare the refractive indices of as-deposited and annealed As_2Se_3 films with those of the parent bulk glasses. They showed that an as-deposited thin film had a lower refractive index than that of the bulk; subsequent annealing of the films increased the refractive index back up to the level of the bulk glass. This illustrates the importance of the thermal history of the glass on its physical structure, and hence on its physical properties such as density and refractive index. In Dantanarayana et al. (2014) we reported the continuous linear refractive index dispersion at ambient temperature of two bulk chalcogenide glasses, AsSe and GeAsSe, over the 0.4–33 μm wavelength range obtained by means of spectroscopic ellipsometry. A two-term Sellmeier equation, with one resonant visible-region absorption and one resonant far-infrared absorption, was determined as sufficient and appropriate for fitting the refractive index dispersion over the wavelength range for which the extinction coefficient was less than 0.0005. The fitting accuracy was better than 0.1%. Nevertheless, the accuracy in measuring the refractive index by means of spectroscopic ellipsometry is inherently limited by surface effects (Poelman and Smet 2003) as a thin contamination layer, oxide layer, or small defects on the surface can all potentially yield different optical constants for the glass.

The method of Swanepoel (1985) was presented to determine the refractive index and thickness of thin films in the transparent region from wavelength values at maxima and minima, only, of the transmission interference fringes. This entails measuring two transmission spectra, one at normal incidence and another at oblique incidence. The Swanepoel method was used by Corrales et al. (1995) to measure the refractive index of an As_2Se_3 thin

film in the 600–2000 nm wavelength region and the method yielded values for refractive index and average thin film thickness to an accuracy of better than 3%. In this paper, an improved Swanepoel method, based on Swanepoel (1985), but modified by the introduction of a Sellmeier dispersion equation in order to improve the applicability of the method to chalcogenide glasses at MIR wavelengths, is introduced. It is used to determine the refractive index dispersion of thin $\text{As}_{40}\text{Se}_{60}$ (at.%, nominal batch composition) and $\text{Ge}_{16}\text{As}_{24}\text{Se}_{15.5}\text{Te}_{44.5}$ (at.%, nominal batch composition) hot-pressed glass films in the MIR spectral region to an accuracy of better than 0.4%. The actual glass compositions measured using scanning electron microscopy energy dispersive X-ray diffraction (SEM-EDX) were found to match the nominal batch compositions to within the ± 0.7 at.% accuracy and precision of the measurements. The present improvements apply to the transparency region of chalcogenide glasses and are distinct from other improvements to the Swanepoel method recently suggested by Jin et al. (2017) who described a tangency point method (TPM) to resolve problems observed when using the Swanepoel method in the strong absorption region.

The remainder of the paper is organised in the following way: in Sect. 2, the preparation of thin film samples of $\text{Ge}_{16}\text{As}_{24}\text{Se}_{15.5}\text{Te}_{44.5}$ and $\text{As}_{40}\text{Se}_{60}$ is introduced, which embraces glass-melting, fibre-drawing, propylamine-etching and hot-pressing. This section also presents experimental measurements of the transmission through the GeAsSeTe and AsSe thin films using Fourier transform infrared spectroscopy (FTIR). Section 3 discusses the appropriate refractive index model to describe the refractive index dispersion of chalcogenide glasses in the MIR spectral region and the basic theory of the improved Swanepoel method to determine the refractive index and thickness of the thin films. Section 4 presents the refractive index and thickness of the thin films obtained from the improved Swanepoel method. The improvements in determining the refractive index dispersion from the improved Swanepoel method are highlighted by comparison with the original approach. The results from the improved method are also compared to the results from ellipsometry, the minimum deviation method and commercial data, in this section. The important conclusions drawn from the study are highlighted in Sect. 5.

2 Sample preparation and FTIR measurements

2.1 Glass melting

In preparing the glass $\text{Ge}_{16}\text{As}_{24}\text{Se}_{15.5}\text{Te}_{44.5}$ and $\text{As}_{40}\text{Se}_{60}$ compositions studied here, the As (7 N purity, Furakawa Denshi) and Se (5 N purity, Materion) elemental precursors were heat-treated under vacuum (10^{-3} Pa) at 310 and 260 °C, respectively, in order to purify them by driving off volatile oxides. Ge (5 N purity, Materion) and Te (5 N purity, Materion) were untreated. The elements were subsequently batched under a nitrogen atmosphere in a MBraun glove-box (≤ 0.1 ppm H_2O and ≤ 0.1 ppm O_2) into a vitreous silica ampoule (Multi-Lab Ltd, UK). Before batching the elements, the vitreous silica ampoule was etched using 40% v/v hydrofluoric acid (HF) and rinsed with deionised water; it was next air and then vacuum baked (under vacuum $\sim 10^{-3}$ Pa) at 1000 °C for 6 h in a vertical furnace (TF105/4.5/IZF, Instron) to drive off physisorbed and chemisorbed water from the inside surface of the silica glass ampoule. After batching, the silica ampoule was sealed (under $\sim 10^{-3}$ Pa vacuum) and placed in a rocking furnace to melt and homogenise the glass, at ~ 750 °C/12 h for the $\text{Ge}_{16}\text{As}_{24}\text{Se}_{15.5}\text{Te}_{44.5}$ composition and at ~ 800 °C/12 h

for the $\text{As}_{40}\text{Se}_{60}$ composition. The melts were quenched and annealed for 1 h at their respective glass transition temperature (T_g) before slowly cooling them down to room temperature. This produced glass rods which were ~ 10 mm in diameter and ~ 70 mm in length.

2.2 Thin film sample preparation

A hot-pressing technique was developed to prepare thin films of chalcogenide glass; this involved the hot-pressing of *circa* 20 mm lengths of fibre, with a nominal diameter of 250 μm , using the hot-press previously described in Fang et al. (2016) (ICTON): Seddon et al. (2006), Abdel-Moneim et al. (2015). The as-annealed preforms (~ 10 mm diameter and ~ 70 mm length) of $\text{Ge}_{16}\text{As}_{24}\text{Se}_{15.5}\text{Te}_{44.5}$ and $\text{As}_{40}\text{Se}_{60}$, prepared as in Sect. 2.1, were drawn into optical fibres using a customised Heathway draw-tower in a 10,000-Class clean-room. The fibres were drawn under a N_2 flow (BOC white-spot) at a viscosity of around $10^{4.5}$ Pa s. The final fibre diameter was 250 ± 10 μm . The outer surface of the fibres was shiny and no defects could be seen by the naked eye. Five $\text{Ge}_{16}\text{As}_{24}\text{Se}_{15.5}\text{Te}_{44.5}$ fibres, each of about 250 μm diameter and 20 mm length, were cleaved from the $\text{Ge}_{16}\text{As}_{24}\text{Se}_{15.5}\text{Te}_{44.5}$ fibre. The five 20 mm lengths of chalcogenide fibre were each immersed in propylamine (Sigma-Aldrich 99 mol.%) for 30 min at room temperature under atmospheric pressure. Subsequently the etched fibres were taken out of the propylamine and were immersed in acetone (99.8%, Sigma Aldrich) for 10 min and subsequently each fibre was individually cleaned carefully using isopropanol (IPA, HPLC grade, Fisher Chemical) with optical lens tissue. A silica glass ampoule (Multi-Lab Ltd, UK) was used as the container for the propylamine-etching; this was rinsed with distilled water and dried under vacuum ($\sim 10^{-3}$ Pa). The five propylamine-etched 20 mm long fibres were then placed on a tungsten carbide plate (800 mm diameter, of flatness 0.08 μm and of surface finish 0.009 μm) surrounded by a 20 μm thick stainless steel shim (Supplier: Hollinbrow Ltd, UK) and then covered by a second tungsten carbide plate. The fibre samples were hot-pressed under vacuum (10^{-4} Pa) at $T_g + 40$ $^\circ\text{C}$ (viscosity $\sim 10^8$ Pa s) with a maximum pressure of 700 N between the two plates. The samples were then annealed at the onset- T_g (175 $^\circ\text{C}$) and allowed to cool with the discs. In order not to damage the samples while opening the press, solvents (acetone and if necessary IPA) were squirted into the gap between the two tungsten carbide plates. $\text{As}_{40}\text{Se}_{60}$ thin films, this time with a 25 μm target (shim) thickness, were also prepared following the same method.

2.3 Optical transmission measurements on the thin-film chalcogenide glass samples using FTIR

A GlobarTM source, KBr beam splitter and DLATGSD301 detector were set up in the FTIR spectrometer (Bruker IFS 66v/s) to measure the interference transmission spectra of the thin films in the wavelength range from 1 to 25 μm ; 25 μm was the maximum wavelength possible with this set-up in the Bruker FTIR. Because of the low efficiency of the KBr beam splitter and the DLATGSD301 detector at wavelengths below 2 μm , clear extrema of interference fringes were only obtained over the wavelength range from 2 to 25 μm .

The $\text{Ge}_{16}\text{As}_{24}\text{Se}_{15.5}\text{Te}_{44.5}$ or $\text{As}_{40}\text{Se}_{60}$ thin film prepared using the hot-pressing technique was mounted on a home-made rotation stage, which was accurate up to 0.1° , installed in the sample compartment of the FTIR spectrometer. In the FTIR spectrometer a He-Ne beam, which was used for alignment, indicated the position of the GlobarTM.

Careful alignment was undertaken to ensure that the axis of rotation went through the surface of the thin film at the focal point of the He–Ne beam and that no lateral displacement of the light took place during rotation. The location of normal incidence was determined by ensuring that equivalent transmission spectra were obtained after rotation through equal angles in a clockwise and anticlockwise sense.

In FTIR thin film transmission measurements, air absorption in the optical path in the mid-infrared region distorted the observed interference fringes, as indicated in Fig. 1. The main absorption bands observed were: CO₂ absorption at around 4.2 and 15 μm and H–O–H absorption at around 2.7 and 6.2 μm (Gibson and MacGregor 2013). A background spectrum was collected immediately before each thin film transmission measurement, without the sample present, with care to ensure that the measurement conditions remained the same; this considerably reduced the effect of air absorption.

Figure 2a, b shows the FTIR interference transmission spectra at normal incidence and at an incident angle of 30° of the Ge₁₆As₂₄Se_{15.5}Te_{44.5} and As₄₀Se₆₀ thin films, respectively. In Fig. 2, the solid curves are the interference fringes obtained from the case of normal incidence and the red curves are from the case of oblique incidence. For the transmission spectra of As₄₀Se₆₀ in Fig. 2b, an obvious material absorption occurred at ~21 μm , which was identified in Maklad et al. (1974) as the second overtone of the fundamental stretching band due to AsSe₃ pyramid units in a As₂Se₃ glass structural matrix itself. This will be discussed further in Sect. 4 with regards to the Sellmeier model adopted in this paper.

3 The theory and analysis of the improved Swanepoel method

3.1 The dispersive refractive index model

Referring to Fig. 2, the method of Swanepoel (1985) was developed to determine the dispersive refractive index and thickness of thin films in the region where $k^2 \ll n^2$ from wavelength values at maxima and minima, only, of the transmission interference fringe. This entailed obtaining two spectra, one at normal incidence and another at oblique incidence. In Swanepoel (1985) the material refractive index was fitted to the dispersive equation given in Eq. (1):

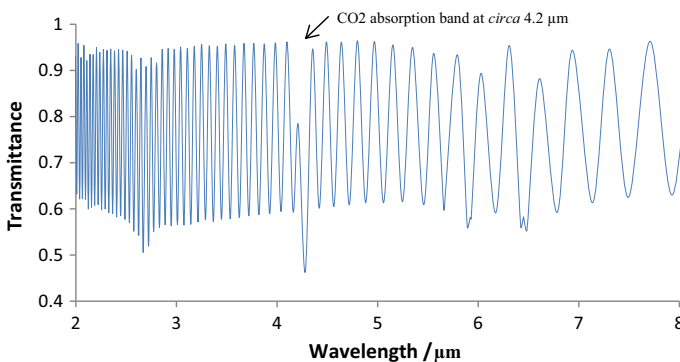


Fig. 1 The transmission spectrum of a Ge₁₆As₂₄Se_{15.5}Te_{44.5} thin film of nominal thickness 20 μm without careful background collection

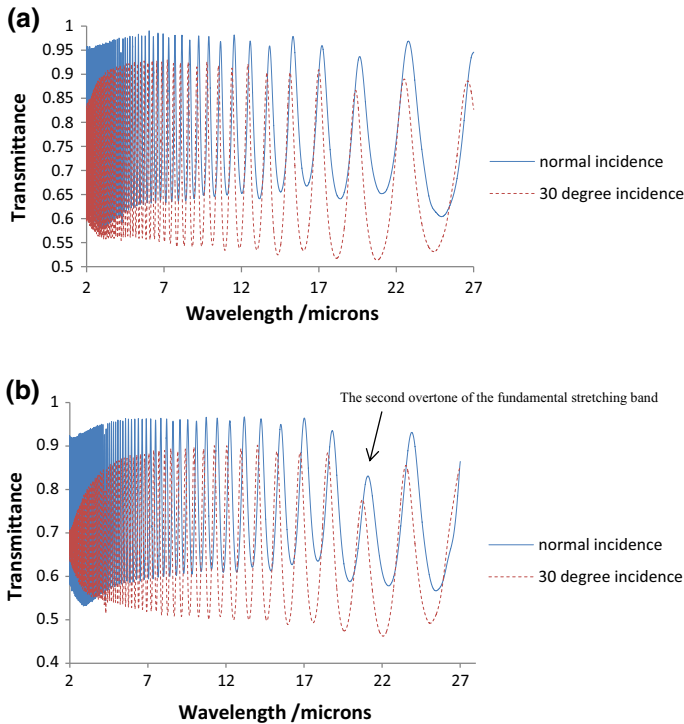


Fig. 2 Transmission spectra for: **a** a 20 μm target thick pressed $\text{Ge}_{16}\text{As}_{24}\text{Se}_{15.5}\text{Te}_{44.5}$ sample at normal incidence (solid curve, blue online) and at an incident angle of 30° (dotted curve, red online) and **b** a 25 μm target thick pressed $\text{As}_{40}\text{Se}_{60}$ sample at normal incidence (solid curve, blue online) and at an incident angle of 30° (dotted curve, red online). (Color figure online)

$$n^2 = A + \frac{B}{\lambda^x} \quad (1)$$

where λ is wavelength and A, B and x are fitting coefficients. The dispersive equation in Eq. (1) is similar to the Cauchy equation, but in order to have a better fit to the refractive index data, the Cauchy model was altered to have an extra fitting parameter x instead of a constant value of wavelength λ . In this paper, we refer to refractive index analysis undertaken using this dispersion equation as ‘the original Swanepoel method’ (Swanepoel 1985). The Cauchy-like model in Eq. (1) assumed that the material band gap, where a resonance in refractive index occurs, is at zero frequency and the model is thus not correct if bandgaps or vibrational absorption bands fall within or close to the frequency range of interest as is the case with chalcogenide glasses (Dantanarayana 2012; Dantanarayana et al. 2014).

In order to extend the Swanepoel method to chalcogenide glasses operating transparently in the MIR spectral region, another refractive index model is needed to replace the Cauchy model as the dispersive equation. Dantanarayana et al. (2014) demonstrated that a two-term Sellmeier model is sufficient to describe the refractive index dispersion of chalcogenide glasses in the transparent region (where $k^2 \ll n^2$). Following Dantanarayana et al. (2014), the transparent region of $\text{As}_{40}\text{Se}_{60}$ and GeAsSe was taken to be where the extinction coefficient k was smaller than 0.0005, which for the two glasses studied in that

paper was the region extending from ~ 0.7 to ~ 30 μm wavelength. Figure 3 shows the absorption coefficient of our $\text{Ge}_{16}\text{As}_{24}\text{Se}_{15.5}\text{Te}_{44.5}$ glass, measured using spectroscopic ellipsometry, from which the transparent region is determined as the wavelength range ~ 1.5 to ~ 29 μm . Unlike the Cauchy method, the Sellmeier model can be used to model materials with one bandgap and one vibrational absorption band in the frequency range of interest. The Sellmeier relation is defined as:

$$n^2(\lambda) = A_0 + \sum_{n=1}^N \frac{A_n \lambda^2}{\lambda^2 - a_n^2} \tag{2}$$

where A_0 and A_n are dimensionless coefficients, N is the number of Sellmeier coefficients (here 2), a_n indicates the N material resonant absorption wavelengths assumed in the model, and λ is wavelength.

Because of the theoretically unbounded nature of the material resonances in the Sellmeier model (*i.e.* the right hand side of Eq. (2) becomes infinite as $\lambda \rightarrow a_n$), the model can only be applied to the non-absorbing spectral region of the material, defined here as the transparent region. In the present paper, the original Swanepoel method was improved by changing the dispersive model from a Cauchy model to a two-term Sellmeier model in order to determine better the thickness and refractive index of thin films of chalcogenide glass in the mid-infrared region.

3.2 The theory of the improved Swanepoel method and analysis

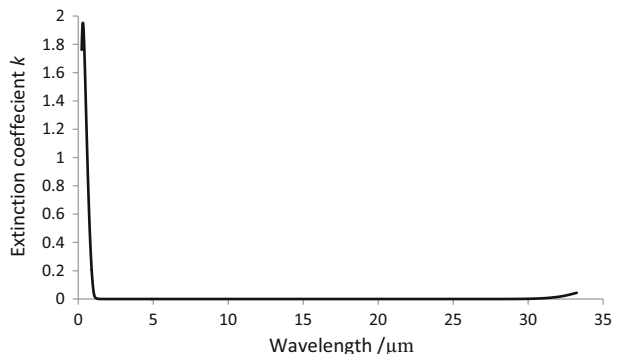
It was assumed that the refractive dispersion is described by a two-term Sellmeier equation [when $N = 2$ in Eq. (2)] and that the refractive index was isotropic. It follows that the spectral dependence of the refractive index could be accurately represented by five constants a_1, a_2, A_0, A_1 and A_2 in the region where the extinction coefficient k satisfied $k^2 \ll n^2$.

For normal incidence on a thin film with thickness d , the wavelengths of the transmission extrema are given by:

$$2n_0d = m\lambda_0 \tag{3}$$

where λ_0 is the wavelength at the maxima or minima of the normal incidence transmission spectrum, n_0 is the refractive index of the material at λ_0 , and m is the order number which has integer values for the maxima and half-integer values for the minima in the case where

Fig. 3 Extinction coefficient k variation with wavelength determined from spectroscopic ellipsometry measurement on a bulk sample of our $\text{Ge}_{16}\text{As}_{24}\text{Se}_{15.5}\text{Te}_{44.5}$ glass



the thin film has no substrate (as in the present study) or the refractive index of thin film is larger than that of the substrate.

Only m and the product n_0d can be determined solely from Eqs. (2) and (3); thus another experimental equation had to be found to determine the other constants. This was obtained by measuring a second transmission spectrum at an angle of incidence $i > 0$, as shown in Fig. 2. The equation for the interference extrema then became (Crawford 1968):

$$2n_i d \cos r = m\lambda_i, \quad (4)$$

where r is the angle of the refraction in the film, λ_i is wavelength at the maxima or minima of the non-normal incidence transmission spectrum, and n_i is the refractive index of the material at λ_i . Equation (4) can be used for a stand-alone thin film (as in the present study) or a film on a transparent substrate.

In Fig. 2a, b, the solid curve is the interference transmission spectrum for normal incidence from 2 to 26 μm . The dotted curve is the spectrum of the same thin film at an incidence angle of 30° . Oblique incidence shifts the interference transmission spectrum to shorter wavelength.

Because the accuracy of the calculation depends on displacement between the interference spectrum for normal incidence and that for oblique incidence, one way to increase the displacement, according to Eq. (3) is by decreasing the sample thickness. For the FTIR thin film measurements, the desired wavelength range was from 2 to 25 μm . In order to have a complete spectrum over this wavelength range, the sample thickness had to be larger than 5 μm for most of chalcogenide glasses (for which n is typically in the range from 2.2 to 3.8). However, the thinner the thickness of the thin films the more difficult it became to collect a complete thin-film sample because of a tendency of the hot-pressed film to stick to the tungsten carbide plates. In our experiments, 20 and 25 μm thick films provided sufficient displacements between the two sets of fringes and yet were robust enough to be readily collected from the hot-press.

Following Swanepoel (1985), the order number m is now considered not to be a discrete-order number but a continuous mathematical variable. The spectrum for normal incidence is shifted towards shorter wavelengths by increasing each order number by an amount Δm , where Δm can be different for each m . The shifting in extrema due to oblique incidence, according to Eq. (4), can be written in terms of normal incidence as:

$$2n_i d = (m + \Delta m)\lambda_i \quad (5)$$

Following Swanepoel (1985) it is noted for later discussion that Eqs. (4), (5), and Snell's law (Eq. 7), yield:

$$\cos r = \frac{m}{m + \Delta m}, \quad (6)$$

using:

$$n_i = \frac{\sin i}{\sin r}, \quad (7)$$

and that it follows from Eq. (3) that two adjacent extrema of the normal-incidence spectrum at wavelengths λ_{01} and λ_{02} , obey

$$m = \frac{n_{01}\lambda_{02}}{2(n_{02}\lambda_{01} - n_{01}\lambda_{02})}. \tag{8}$$

Substitution Eq. (2) into Eq. (3) yields:

$$m^2\lambda_0^2 = A + \frac{B\lambda_0^2}{\lambda_0^2 - a_1^2} + \frac{C\lambda_0^2}{\lambda_0^2 - a_2^2}, \tag{9}$$

where $A = 4ad^2$, $B = 4bd^2$ and $C = 4cd^2$. The order numbers m at each extremum are required before the values of A , B , C , a_1 and a_2 in the two-term Sellmeier fit can be determined.

In Swanepoel (1985) the values of m were found by introducing an intermediate quantity M as

$$M = \frac{\lambda_{02}}{2(\lambda_{01} - \lambda_{02})}, \tag{10}$$

where $M \geq m$. $M = m$ in the non-dispersive case. In the dispersive case, the dispersion of M was described by the approximate form:

$$M = \frac{C_s}{\lambda_0} \left(1 + \frac{D_s}{\lambda_0^y} \right) \tag{11}$$

where C_s , D_s and y are fitting parameters. It will be shown in Sect. 4 that this approach works well for determining m in the present studies. The dispersion of M can also be described using a Sellmeier-inspired fitting of the form:

$$M = \frac{E}{\lambda_0} \left(1 + \frac{F}{1 - \left(\frac{b_1}{\lambda_0}\right)^2} + \frac{G}{1 - \left(\frac{b_2}{\lambda_0}\right)^2} \right), \tag{12}$$

where E , F , G , b_1 and b_2 are fitting parameters which can then be used to find values of m ($\leq M$) where, at each extremum wavelength λ_o , m takes an integer value close to transmission maxima and half integer values of m close to transmission minima

Substitution Eq. (2) into Eq. (5), using Eq. (9), and solving for Δm yields:

$$\Delta m = \left[m^2 \frac{\lambda_0^2}{\lambda_i^2} + \frac{B}{\lambda_i^2} \left(\frac{1}{1 - \left(\frac{a_1}{\lambda_i}\right)^2} - \frac{1}{1 - \left(\frac{a_1}{\lambda_0}\right)^2} \right) + \frac{C}{\lambda_i^2} \left(\frac{1}{1 - \left(\frac{a_2}{\lambda_i}\right)^2} - \frac{1}{1 - \left(\frac{a_2}{\lambda_0}\right)^2} \right) \right]^{1/2} - m. \tag{13}$$

The value of n_i at each wavelength can be calculated using Eqs. (13), (6) and (7).

Since m increases by 1/2 for each successive extremum described by Eq. (5), the value of d , film thickness, can subsequently be determined. If the order the first extremum, m_1 , is considered to be at the long-wavelength end, Eq. (5) can be written for the successive extreme as described in an earlier paper of Swanepoel (1983), as:

$$\left(\frac{L}{2} + \Delta m \right) = 2d \frac{n_i}{\lambda_i} - m_1, \tag{14}$$

where m_1 is the first order number, $L = 0, 1, 2, 3, \dots$. Using $(\frac{L}{2} + \Delta m)$ as the dependent variable and $\frac{n_i}{\lambda_i}$ as the independent variable, a straight line can be plotted whose gradient can be used to determine d .

With d and m known, the final values of refractive index at the wavelength of extrema can be determined from Eq. (3). The two-term Sellmeier model of Eq. (2) is then used to fit the final values of refractive index.

4 Results and discussion

The interference transmission spectra of the $\text{Ge}_{16}\text{As}_{24}\text{Se}_{15.5}\text{Te}_{44.5}$ and the $\text{As}_{40}\text{Se}_{60}$ thin films are shown respectively in Fig. 2a, b. The solid curves in Fig. 2 represent the interference transmission spectrum for normal incidence whereas the dotted spectrum is that for an incidence angle of 30° . Because the accuracy of the calculation depends on $(\lambda_0 - \lambda_i)$, the angle of non-normal incidence should be large enough to get sufficient displacement but not so large that the lateral spreading of the beam provides errors in the case of non-uniform films. No particular significance should be attached to the actual values of transmission of the oblique angle of incidence spectrum (dotted curve, red online) because the effects of polarization can influence its magnitude for large angles of incidence (Fowles 1975). Another method to get sufficient displacement is to decrease the thickness of thin films. As discussed in Sect. 3.2, decreasing the thickness of the thin film will result in increasing difficulties in collecting complete samples after the hot-pressing. Thin films having nominal thicknesses of 20 and 25 μm provide sufficient displacements between two fringes and yet were strong enough to be collected.

Since the interference fringes below 2.85 μm are influenced by atmospheric water absorption at wavelengths around 2.7 μm and the displacements $(\lambda_0 - \lambda_i)$ were relatively small, which led to errors in determining the thickness of the thin film as well as of the refractive index, the extrema at wavelengths below 2.85 μm were not selected when determining the thickness of the thin film. Some wavelengths of the extrema of $\text{Ge}_{16}\text{As}_{24}\text{Se}_{15.5}\text{Te}_{44.5}$ and $\text{As}_{40}\text{Se}_{60}$ thin films are listed in Tables 1 and 2 as λ_0 for normal incidence and as λ_i for oblique incidence. These values could be determined to an accuracy of 1 nm from the transmission spectra, sufficient to get a meaningful result (Swanepoel 1985).

The values of M that were calculated from Eq. (10), using the wavelengths at which adjacent extrema occur at normal incidence, are shown in Table 2. These values were fitted to Eq. (12) iterating b_1 in steps of 0.0001 μm from 0 to 1.5 μm and b_2 in steps of 0.01 μm from 32 to 100 μm for $\text{Ge}_{16}\text{As}_{24}\text{Se}_{15.5}\text{Te}_{44.5}$, since the resonance wavelength b_1 and b_2 must be initially placed outside the transparent window fitting region to avoid the Sellmeier model becoming unbounded (Dantanarayana et al. 2014). For AsSe , b_1 was varied from 0 to 0.7 μm in steps of 0.0001 μm and b_2 was iterated from 30 to 100 μm in steps of 0.01 μm . A good fit was obtained for both $\text{Ge}_{16}\text{As}_{24}\text{Se}_{15.5}\text{Te}_{44.5}$ and $\text{As}_{40}\text{Se}_{60}$ yielding estimates for m at each extrema wavelength λ_0 , termed m_y following the notation of Swanepoel (1985), as

$$m_y \lambda_0 = 123.20 + \frac{16.19}{1 - \left(\frac{1.22}{\lambda_0}\right)^2} + \frac{1.04 \times 10^{-6}}{1 - \left(\frac{100.00}{\lambda_0}\right)^2} \quad \text{for } \text{Ge}_{16}\text{As}_{24}\text{Se}_{15.5}\text{Te}_{44.5} \quad (15a)$$

Table 1 Calculations of refractive index of Ge₁₆As₂₄Se_{15.5}Te_{44.5} (GeAsSeTe) and As₄₀Se₆₀ (AsSe) thin films from the improved Swanepoel method

Thin film	λ_0	λ_i	M	m_y	m	Δm	n_i	n	$n_{\text{ellipsometry}}$	
GeAsSeTe	22.786	22.509	6.1	6.1	6	0.0770	3.150	3.131	3.1255	
	21.052	20.760	7.0	6.6	6.5	0.0944	2.967	3.134	3.1371	
	19.635	19.370	7.3	7.1	7	0.0985	3.011	3.148	3.1447	
	18.381	18.136	7.3	7.6	7.5	0.1036	3.040	3.158	3.1503	
	17.203	16.996	8.2	8.1	8	0.0994	3.201	3.152	3.1549	
	16.217	16.013	8.7	8.6	8.5	0.1102	3.136	3.157	3.1583	
								
	3.042	3.005	46.7	46.8	46	0.5650	3.214	3.205	3.2065	
	3.010	2.974	48.3	47.4	46.5	0.5669	3.227	3.205	3.2072	
	2.979	2.943	47.7	47.9	47	0.5864	3.195	3.206	3.2078	
	2.948	2.912	48.4	48.4	47.5	0.5875	3.209	3.207	3.2085	
	2.918	2.883	49.0	49.0	48	0.5944	3.207	3.208	3.2092	
	2.888	2.853		49.5	48.5	0.6008	3.206	3.208	3.2099	
	d = 21.83 μm	$n_{3.1\mu\text{m}}$ from the minimum deviation method = 3.1920								
	AsSe	23.896	23.5169	7.5	7.3	7	0.1213	2.720	2.710	–
22.411		22.0428	8.0	7.8	7.5	0.1333	2.687	2.723	–	
21.087		20.7323	8.6	8.2	8	0.1440	2.671	2.733	–	
19.934		19.5787	8.3	8.7	8.5	0.1611	2.604	2.745	–	
18.803		18.5132	9.7	9.2	9	0.1466	2.804	2.742	–	
17.880		17.5843	9.8	9.7	9.5	0.1655	2.714	2.752	–	
...		...								
3.040		2.991	57.8	57.6	57	0.9311	2.800	2.807	–	
3.014		2.966	57.3	58.1	57.5	0.9341	2.808	2.807	–	
2.988		2.941	58.4	58.6	58	0.9296	2.826	2.807	–	
2.962		2.916	59.5	59.1	58.5	0.9392	2.824	2.808	–	
2.938		2.891	60.7	59.6	59	0.9554	2.812	2.808	–	
2.914		2.867	–	60.1	59.5	0.9717	2.800	2.808	–	
d = 30.88 μm		$n_{3.1\mu\text{m}}$ from the minimum deviation method = 2.7972								

$$m_y \lambda_0 = 142.60 + \frac{519.80}{1 - \left(\frac{0.70}{\lambda_0}\right)^2} + \frac{5.33 \times 10^{-6}}{1 - \left(\frac{100.00}{\lambda_0}\right)^2} \quad \text{for As}_{40}\text{Se}_{60} \quad (15b)$$

The values of M from Eq. (10) and m_y from Eqs. (15a, 15b) are shown in Table 1, together with the actual value of m deduced.

The original Swanepoel approach to determining M, summarised by Eq. (11), yields

$$M \lambda_0 = \frac{164.3268}{\lambda_0^{3.6}} + 139.6986 \quad \text{for Ge}_{16}\text{As}_{24}\text{Se}_{15.5}\text{Te}_{44.5} \quad (16a)$$

Table 2 Calculations of the refractive index of Ge₁₆As₂₄Se_{15.5}Te_{44.5} (GeAsSeTe) and As₄₀Se₆₀ (AsSe) thin films from the original Swanepoel method

Thin film	$\hat{\lambda}_0$	$\hat{\lambda}_i$	M	m_y	m	Δm	n_i	n	$n_{\text{ellipsometry}}$
GeAsSeTe	22.786	22.509	6.1	6.1	6	0.0740	3.212	3.158	3.1255
	21.052	20.760	7.0	6.6	6.5	0.0916	3.010	3.159	3.1371
	19.635	19.370	7.3	7.1	7	0.0963	3.045	3.159	3.1447
	18.381	18.136	7.3	7.6	7.5	0.1017	3.067	3.160	3.1503
	17.203	16.996	8.2	8.1	8	0.0980	3.224	3.160	3.1549
	16.217	16.013	8.7	8.6	8.5	0.1089	3.154	3.161	3.1583
	...								
	3.042	3.005	46.7	45.9	46	0.5660	3.217	3.206	3.2065
	3.010	2.974	48.3	46.4	46.5	0.5673	3.230	3.206	3.2072
	2.979	2.943	47.7	46.9	47	0.5853	3.198	3.207	3.2078
	2.948	2.912	48.4	47.4	47.5	0.5862	3.212	3.207	3.2085
	2.918	2.883	49.0	47.9	48	0.5930	3.210	3.208	3.2092
	2.888	2.853		48.4	48.5	0.5993	3.210	3.209	3.2099
	d = 21.84 μm	$n_{3.1\mu\text{m}}$ from the minimum deviation method = 3.1920							
AsSe	23.896	23.5169	7.5	7.3	7	0.1131	2.815	2.761	–
	22.411	22.0428	8.0	7.8	7.5	0.1258	2.765	2.761	–
	21.087	20.7323	8.6	8.3	8	0.1371	2.735	2.761	–
	19.934	19.5787	8.3	8.7	8.5	0.1546	2.657	2.761	–
	18.803	18.5132	9.7	9.3	9	0.1415	2.853	2.762	–
	17.880	17.5843	9.8	9.7	9.5	0.1604	2.755	2.762	–
	...								
	3.040	2.991	57.8	57.2	57	0.9394	2.788	2.797	–
	3.014	2.966	57.3	57.7	57.5	0.9323	2.796	2.797	–
	2.988	2.941	58.4	58.2	58	0.9379	2.814	2.798	–
	2.962	2.916	59.5	58.7	58.5	0.9475	2.812	2.798	–
	2.938	2.891	60.7	59.2	59	0.9639	2.800	2.798	–
	2.914	2.867	–	59.7	59.5	0.9803	2.788	2.799	–
	d = 30.98 μm	$n_{3.1\mu\text{m}}$ from the minimum deviation method = 2.7972							

$$M\lambda_0 = \frac{930.3893}{\lambda_0^{3.6}} + 173.9862 \quad \text{for As}_{40}\text{Se}_{60} \tag{16b}$$

As in Swanepoel (1985) the values of m_y are calculated from the first terms on the right hand side of Eqs. (16a) and (16b), and are shown in Table 2 along with the connected values of m . From Tables 1 and 2, it can be seen that both of these methods are able to determine the actual order number m of the fringes in Fig. 2.

The actual values of m are used in Eq. (9), iterating a_1 in step of 0.0001 μm from 0 to 1.5 μm and a_2 in step of 0.01 μm from 32 to 100 μm for Ge₁₆As₂₄Se_{15.5}Te_{44.5}. For As₄₀Se₆₀, b_1 was iterated from 0 to 0.7 μm in step of 0.0001 μm and b_2 was iterated from 30 to 100 μm in step of 0.01 μm . The best fit was obtained for $a_1 = 0.4051$ and $a_2 = 41.85$

in the case of $\text{Ge}_{16}\text{As}_{24}\text{Se}_{15.5}\text{Te}_{44.5}$, which is shown in Fig. 3a and $a_1 = 0.6584$ and $a_2 = 58.30$ in the case of $\text{As}_{40}\text{Se}_{60}$ as shown in Fig. 3c yielding:

$$m^2\lambda_0^2 = 1.118 + \frac{1.924 \times 10^4 \lambda^2}{\lambda^2 - 0.4051^2} + \frac{1353\lambda^2}{\lambda^2 - 41.85^2} \quad \text{for } \text{Ge}_{16}\text{As}_{24}\text{Se}_{15.5}\text{Te}_{44.5} \quad (17a)$$

$$m^2\lambda_0^2 = 2.425 \times 10^4 + \frac{5524\lambda^2}{\lambda^2 - 0.6584^2} + \frac{8832\lambda^2}{\lambda^2 - 58.30^2} \quad \text{for } \text{As}_{40}\text{Se}_{60} \quad (17b)$$

From the original Swanepoel method, the best fit was obtained when $x = 1$ yielding:

$$m^2\lambda_0^2 = \frac{2.028 \times 10^3}{\lambda^1} + 1.893 \times 10^4 \quad \text{for } \text{Ge}_{16}\text{As}_{24}\text{Se}_{15.5}\text{Te}_{44.5} \quad (18a)$$

$$m^2\lambda_0^2 = \frac{3.506 \times 10^3}{\lambda^1} + 2.901 \times 10^4 \quad \text{for } \text{As}_{40}\text{Se}_{60} \quad (18b)$$

For $\text{Ge}_{16}\text{As}_{24}\text{Se}_{15.5}\text{Te}_{44.5}$, the best fitting from the original Swanepoel method is shown in Fig. 4c. The value of R^2 (correlation coefficient) is 0.8997 and MSE (mean squares error) is 3.584×10^3 . After the improvement of the method, the fitting is shown in Fig. 4a

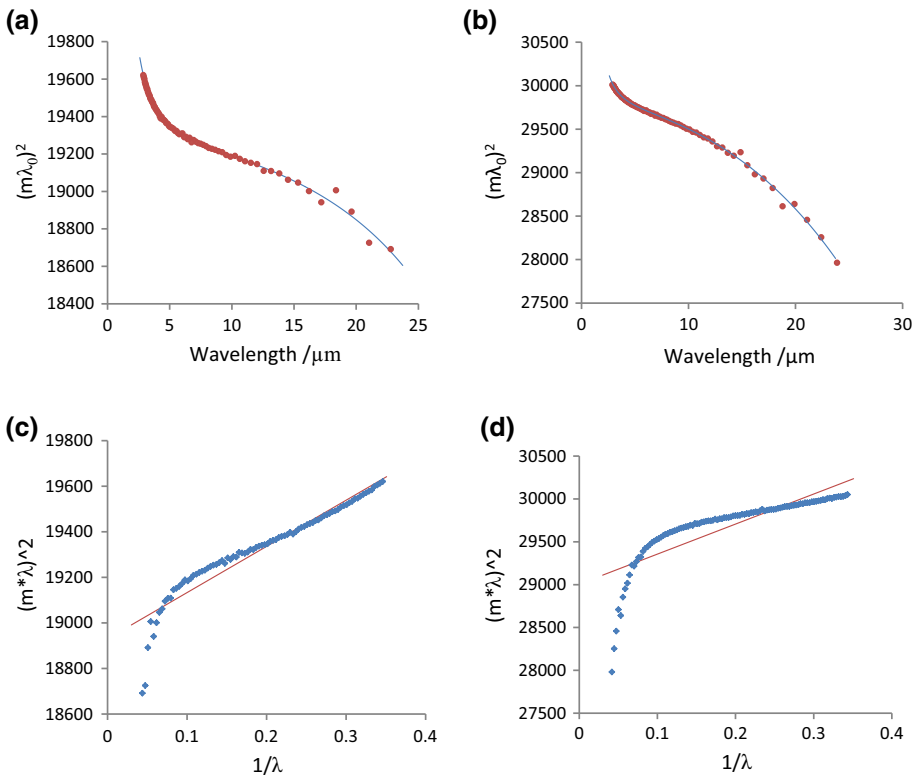


Fig. 4 a, b Best fit to Eq. (9) in the improved Swanepoel method, Eqs. (17a, 17b), for a $\text{Ge}_{16}\text{As}_{24}\text{Se}_{15.5}\text{Te}_{44.5}$, b $\text{As}_{40}\text{Se}_{60}$; c, d best fit to the experimental data using the original Swanepoel method, Eqs. (18a, 18b), c $\text{Ge}_{16}\text{As}_{24}\text{Se}_{15.5}\text{Te}_{44.5}$, d $\text{As}_{40}\text{Se}_{60}$

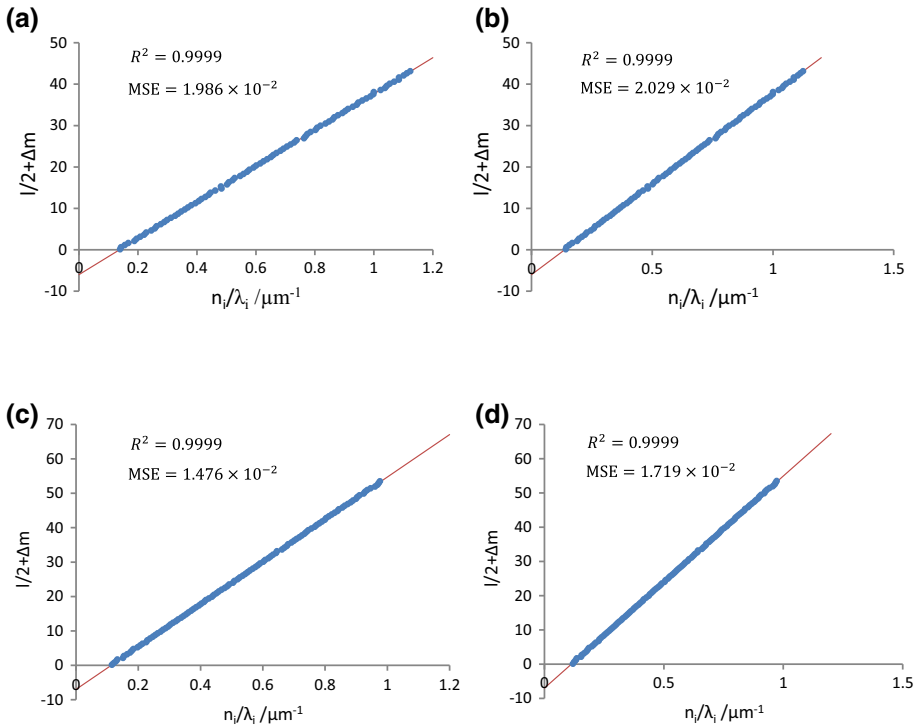


Fig. 5 Plot of $1/2 + \Delta m$ as a function of n_i/λ_i for: **a** $\text{Ge}_{16}\text{As}_{24}\text{Se}_{15.5}\text{Te}_{44.5}$ thin film from improved Swanepoel method; **b** $\text{Ge}_{16}\text{As}_{24}\text{Se}_{15.5}\text{Te}_{44.5}$ thin film from the original method; **c** $\text{As}_{40}\text{Se}_{60}$ thin film from improved Swanepoel method and **d** $\text{As}_{40}\text{Se}_{60}$ thin film from the original Swanepoel method to determine the film thickness d

with $R^2 = 0.9954$ and $\text{MSE} = 1.621 \times 10^2$. Applying the original Swanepoel method to $\text{As}_{40}\text{Se}_{60}$, R^2 of the best fit is 0.6702 and the MSE is 4.686×10^4 , as shown in Fig. 4d. From Fig. 4b, the best fit from the improved Swanepoel method yields $R^2 = 0.9980$ and $\text{MSE} = 2.858 \times 10^2$. The poor fits from the original Swanepoel method indicate that the original dispersive model is not appropriate to describe the refractive index dispersion of chalcogenide thin films in the mid-infrared region. In contrast, good quality fitting to the $m\lambda_0$ data, as in Eq. (9), was obtained by using a two-term Sellmeier model as the dispersive equation.

Δm was calculated from Eq. (13) and n_i was calculated from Eqs. (6) and (7). The results of Δm and n_i for $\text{Ge}_{16}\text{As}_{24}\text{Se}_{15.5}\text{Te}_{44.5}$ and $\text{As}_{40}\text{Se}_{60}$ from the improved method are shown in Table 1. Figure 5 shows a plot of $1/2 + \Delta m$ as a function of n_i/λ_i ; Eq. (14) shows that the gradient of this straight line plot is $2d$. The slope of the straight line is $43.66 \mu\text{m}$ for $\text{Ge}_{16}\text{As}_{24}\text{Se}_{15.5}\text{Te}_{44.5}$ and $61.76 \mu\text{m}$ for $\text{As}_{40}\text{Se}_{60}$, yielding values for d of $d = 21.83 \mu\text{m}$ (target thickness: $20 \mu\text{m}$) and $d = 30.88 \mu\text{m}$ (target thickness: $25 \mu\text{m}$), respectively. The difference between the calculated thickness and the target thickness can be attributed to the quality of the shims, short hot-pressing time or the high glass-melt viscosity during the hot pressing.

The results of Δm and n_i for $\text{Ge}_{16}\text{As}_{24}\text{Se}_{15.5}\text{Te}_{44.5}$ and $\text{As}_{40}\text{Se}_{60}$ from the original Swanepoel are shown in Table 2. The plots of Eq. (14) are shown in Fig. 5b for

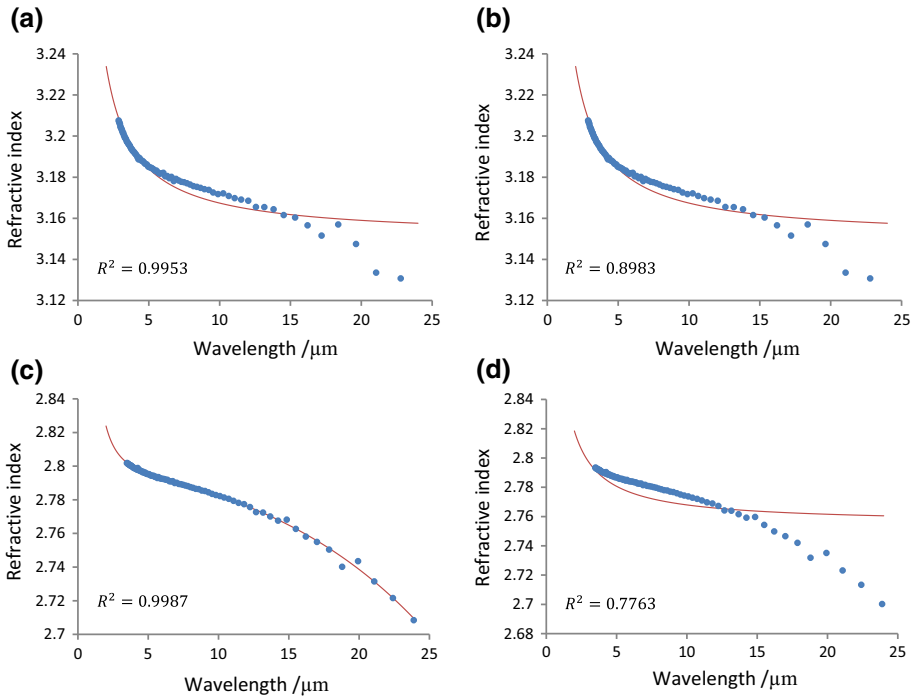


Fig. 6 The fits to the final refractive index values (temperature of the measurements: $23.1 \pm 0.5 \text{ }^\circ\text{C}$) of: **a** $\text{Ge}_{16}\text{As}_{24}\text{Se}_{15.5}\text{Te}_{44.5}$ from the improved Swanepoel method; **b** $\text{Ge}_{16}\text{As}_{24}\text{Se}_{15.5}\text{Te}_{44.5}$ from the original Swanepoel method; **c** $\text{As}_{40}\text{Se}_{60}$ from the improved Swanepoel method and **d** $\text{As}_{40}\text{Se}_{60}$ from the original Swanepoel method

$\text{Ge}_{16}\text{As}_{24}\text{Se}_{15.5}\text{Te}_{44.5}$ and Fig. 5d for $\text{As}_{40}\text{Se}_{60}$. The calculated thickness of GeAsSeTe and AsSe are 21.84 and 30.98 μm , respectively.

From Fig. 5a, b, the MSE from the improved method for the $\text{Ge}_{16}\text{As}_{24}\text{Se}_{15.5}\text{Te}_{44.5}$ measurement was 4.302×10^{-4} lower than that from the original Swanepoel method. The MSE from the improved method for AsSe was 2.425×10^{-3} lower than that from the original method, as shown in Fig. 5c, d. Although the quality of the line fitting was similar, the values of Δm from the original method were obtained from the poor fitting in Fig. 4c, which would have led to an error in determining the film thickness d . In the case of $\text{Ge}_{16}\text{As}_{24}\text{Se}_{15.5}\text{Te}_{44.5}$, the thickness determination was better by 0.01 μm in the improved method, which would have led to ~ 0.001 difference in refractive index. In the case of $\text{As}_{40}\text{Se}_{60}$, the observed difference of thickness was 0.1 μm which would have led to a refractive index difference of ~ 0.009 .

With d and m known, the final values of refractive index at the wavelength of extremes, which are shown in Table 1, could be determined from Eq. (3). The fits of these final values to Eq. (3) from the improved Swanepoel method are shown in Fig. 6a, b, which yield:

$$n^2 = 5.259 + \frac{4.837\lambda^2}{\lambda^2 - 0.5771^2} + \frac{0.7964\lambda^2}{\lambda^2 - 43.72^2} \quad \text{for } \text{Ge}_{16}\text{As}_{24}\text{Se}_{15.5}\text{Te}_{44.5}$$

$$n^2 = 3.463 + \frac{4.341\lambda^2}{\lambda^2 - 0.3920^2} + \frac{2.124\lambda^2}{\lambda^2 - 56.31^2} \quad \text{for As}_{40}\text{Se}_{60}$$

In our previous study of a Sellmeier refractive index model fit to $\text{As}_{40}\text{Se}_{60}$ ellipsometry data (Dantanarayana et al. 2014), several different sets of Sellmeier coefficients could be obtained depending on the choice of a_n parameters in the Sellmeier fit. We believe that it is important that the two-term Sellmeier model lends itself to a physical interpretation as this could open the way to the model being a predictive tool. In our previous work, in the two-term Sellmeier the a_1 coefficient was proposed to be linked to the optical bandgap and a_2 proposed to be associated with vibrational band resonant fundamental absorption. The value of a_2 in Dantanarayana et al. (2014) was $41.395 \mu\text{m}$ which fits well with the position of the fundamental As–Se stretching band calculated to occur at $41.7 \mu\text{m}$ (Maklad et al. 1974). Performing a fit to the present experimental data for the refractive index of $\text{As}_{40}\text{Se}_{60}$, but now fixing the value of a_2 to that which was used in Dantanarayana et al. (2014), yields:

$$n^2 = 4.196 + \frac{3.602\lambda^2}{\lambda^2 - 0.43834^2} + \frac{0.975\lambda^2}{\lambda^2 - 41.395^2} \quad \text{for As}_{40}\text{Se}_{60}$$

with $R^2 = 0.9975$. Compared to the best fit in Fig. 6c, the R^2 decreases from 0.9987 to 0.9975. The difference between the two fits may be attributed to the limited experimental wavelength region (2–25 μm) and the effect of the material absorption [at 20.8 μm —which is the first overtone of the As–Se fundamental stretching vibrational absorption at 41.7 μm (Maklad et al. 1974)]. For the $\text{Ge}_{16}\text{As}_{24}\text{Se}_{15.5}\text{Te}_{44.5}$ glass no bandgap information is available, and no obvious material absorption was noticed in the transmission spectrum and thus a best Sellmeier fit to the experimental data is presented.

The fits of these final values to Eq. (3) from the original Swanepoel method are shown in Fig. 6b, d, which yield:

$$n^2 = \frac{1.064}{\lambda^1} + 9.926 \quad \text{for Ge}_{16}\text{As}_{24}\text{Se}_{15.5}\text{Te}_{44.5}$$

$$n^2 = \frac{0.7057}{\lambda^1} + 7.591 \quad \text{for As}_{40}\text{Se}_{60}$$

For the $\text{Ge}_{16}\text{As}_{24}\text{Se}_{15.5}\text{Te}_{44.5}$ thin film, the Sellmeier dispersive equation introduced in this paper also provided better curve fitting to the refractive index data than the original dispersive equation, as shown in Fig. 6a, b. The value of R^2 improved from 0.8983 to 0.9953. For the $\text{As}_{40}\text{Se}_{60}$ thin film, the fit from the improved Swanepoel method is far better than that from the original method, as shown in Fig. 6c, d. In Fig. 6b, d, it is obvious that the original dispersive equation could not encompass the entire transparent window of chalcogenide glasses. The results confirm the findings of Dantanarayana et al. (2014) that a two-term Sellmeier model, with one resonant absorption in the glass optical bandgap region and one resonant absorption in the fundamental absorption spectral region in the mid-infrared, is sufficient for fitting the refractive index dispersion across the transparent window of each glass.

The refractive indices of $\text{Ge}_{16}\text{As}_{24}\text{Se}_{15.5}\text{Te}_{44.5}$ and $\text{As}_{40}\text{Se}_{60}$ from the present thin film measurements, a prism minimum deviation measurement (Fang et al. 2016) and ellipsometry are shown in Fig. 7. All the $\text{Ge}_{16}\text{As}_{24}\text{Se}_{15.5}\text{Te}_{44.5}$ measurements were made on glass samples from the same glass-melt-batch. The prism and thin film measurements for

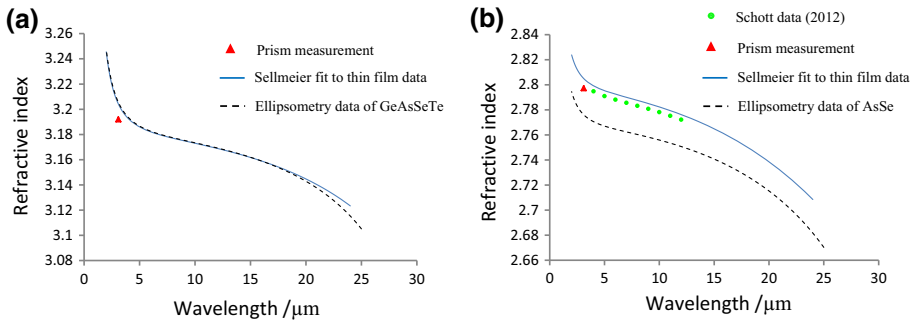


Fig. 7 Sellmeier fit to the final refractive index values of **a** $\text{Ge}_{16}\text{As}_{24}\text{Se}_{15.5}\text{Te}_{44.5}$ and **b** $\text{As}_{40}\text{Se}_{60}$ from FTIR thin film measurements comparing to the data from minimum deviation measurement, ellipsometry and Schott (2013)

$\text{As}_{40}\text{Se}_{60}$ were also made on glass from the same glass-melt-batch but the ellipsometry measurements are those reported in Dantanarayana et al. (2014) and were made on $\text{As}_{40}\text{Se}_{60}$ glass from a different glass-melt-batch. The minimum deviation method in our laboratory is able to determine the refractive index of chalcogenide prisms with a standard deviation of less than 0.001; we take these results as our benchmark value. From Fig. 7a, the difference in refractive index for the $\text{Ge}_{16}\text{As}_{24}\text{Se}_{15.5}\text{Te}_{44.5}$ from the thin film measurements and from the minimum deviation measurements is 0.0119 (0.37%) at a wavelength of 3.1 μm , which might be attributed to their different thermal history (that is, the difference in quenching and annealing of the bulk glass to make the prism and after hot-pressing to make the thin film). In contrast, since the thin film and ellipsometry sample of $\text{Ge}_{16}\text{As}_{24}\text{Se}_{15.5}\text{Te}_{44.5}$ were actually both hot-pressed in a similar manner, which provided a similar thermal history, this provides understanding of why the error in refractive index between them is less than 0.17% from 2 to 25 μm . For $\text{As}_{40}\text{Se}_{60}$, the difference in refractive index between the thin film measurements and ellipsometry is greater than that for the $\text{Ge}_{16}\text{As}_{24}\text{Se}_{15.5}\text{Te}_{44.5}$, but is still less than 1.05% from 2 to 25 μm , and is subject to unintentional compositional differences between the different glass batches which were prepared and then melted independently of one another. From Fig. 7b, the difference in refractive index between the thin film measurements and the prism minimum deviation measurements is 0.0079 (0.28%) at a wavelength of 3.1 μm , and the difference in the refractive index from the improved Swanepoel method compared to the commercial Schott data (Schott 2013) is less than 0.0043. Repeated measurements showed that the refractive index dispersion is determined by the improved method with a standard deviation of less than 0.0027 for the $\text{As}_{40}\text{Se}_{60}$ thin films and less than 0.002 for the $\text{Ge}_{16}\text{As}_{24}\text{Se}_{15.5}\text{Te}_{44.5}$ thin films.

The Swanepoel method in both the original and improved forms is sensitive to the calculated sample thickness, as indicated by Eq. (3). The surfaces of the thin films of $\text{Ge}_{16}\text{As}_{24}\text{Se}_{15.5}\text{Te}_{44.5}$ and $\text{As}_{40}\text{Se}_{60}$ produced were both not perfect. However, according to (Swanepoel 1985) these kinds of glass surface undulation and glass surface defects (so long as they are limited in size relative to the wavelength of the light) do not affect the wavelength values of the extrema and hence the method used still yields correct and accurate values for refractive index and thickness.

5 Conclusions

A hot-pressing technique was used to fabricate chalcogenide glass thin films of 20 and 25 μm target thickness from fibres. The characteristic interference fringes in the spectral transmission of these thin films were obtained over the wavelength range from 2 to 25 μm by FTIR spectroscopy. The Swanepoel method (Swanepoel 1985) was modified to include a two-term Sellmeier model as the dispersive equation and was successfully applied to determine the refractive index of $\text{Ge}_{16}\text{As}_{24}\text{Se}_{15.5}\text{Te}_{44.5}$ and $\text{As}_{40}\text{Se}_{60}$ thin films over the wavelength range from 2 to 25 μm to an accuracy of better than 0.4%. It was shown that the original Swanepoel method (Swanepoel 1985) failed to correctly determine the refractive index dispersion of the chalcogenide glasses studied in the MIR spectral region because it uses an inappropriate Cauchy-like dispersive equation. The average thicknesses of the non-uniform thin films were also determined by the improved Swanepoel method presented.

Acknowledgements The authors are grateful to the Naval Research Laboratory (Washington D. C. USA) for their support in providing the ICL used in this work.

Open Access This article is distributed under the terms of the Creative Commons Attribution 4.0 International License (<http://creativecommons.org/licenses/by/4.0/>), which permits unrestricted use, distribution, and reproduction in any medium, provided you give appropriate credit to the original author(s) and the source, provide a link to the Creative Commons license, and indicate if changes were made.

References

- Abdel-Moneim, N.S., Mellor, C.J., Benson, T.M., Furniss, D., Seddon, A.B.: Fabrication of stable, low loss optical loss rib-waveguides via embossing of sputtered chalcogenide glass-film on glass-chip. *Opt. Quantum Electron.* **47**(2), 351–361 (2015)
- Carlie, N., Anheier, N., Qiao, H., Bernacki, B., Phillippe, M., Petit, L., Musgraves, J., Richardson, K.: Measurement of the refractive index dispersion of As_2Se_3 bulk glass and thin films prior to and after laser irradiation and annealing using prism coupling in the near- and mid-infrared spectral range. *Rev. Sci. Instrum.* **82**, 053103-1–053103-7 (2011)
- Corrales, C., Ramírez-Malo, J., Fernández-Peña, J., Villares, P., Swanepoel, R., Márquez, E.: Determining the refractive index and average thickness of AsSe semiconducting glass films from wavelength measurement only. *Appl. Opt.* **34**, 7907–7913 (1995)
- Crawford, F.S.: *Waves*, p. 182. McGraw-Hill, New York (1968)
- Dantanarayana, H.: Application of TLM for optical micro-resonators. Ph.D. thesis, Faculty of Engineering, The University of Nottingham, Nottingham (2012)
- Dantanarayana, H.G., Abdel-Moneim, N., Tang, Z., Sojka, L., Sujecki, S., Furniss, D., Seddon, A.B., Kubat, I., Bang, O., Benson, T.M.: Refractive index dispersion of chalcogenide glasses for ultra-high numerical-aperture fiber for mid-infrared supercontinuum generation. *Opt. Mater. Express* **4**(7), 1444–1455 (2014)
- Falconi, M.C., Palma, G., Starecki, F., Nazabal, V., Troles, J., Taccheo, S., Ferrari, M., Prudenzano, F.: Design of an efficient pumping scheme for mid-IR $\text{Dy}^{3+} : \text{Ga}_5\text{Ge}_{20}\text{Sb}_{10}\text{S}_{65}$ PCF fiber laser. *IEEE Photonics Technol. Lett.* **28**(18), 1984–1987 (2016)
- Falconi, M.C., Palma, G., Starecki, F., Nazabal, V., Troles, J., Adam, J., Taccheo, S., Ferrari, M., Prudenzano, F.: Dysprosium-doped chalcogenide master oscillator power amplifier (MOPA) for mid-IR Emission. *J. Lightwave Technol.* **35**(2), 265–273 (2017)
- Fang, Y., Sójka, L., Jayasuriya, D., Furniss, D., Tang, Z.Q., Markos, C., Sujecki, S., Seddon, A.B., Benson, T.M.: Characterising refractive index dispersion in chalcogenide glasses. In: Proceedings of 18th International Conference on Transparent Optical Networks (2016)
- Fowles, G.R.: *Introduction to Modern Optics*, p. 44. Holt, Rinhart and Winston, New York (1975)
- Gibson, D., MacGregor, C.: A novel solid state non-dispersive infrared CO_2 gas sensor compatible with wireless and portable deployment. *Sensors* **13**(6), 7079–7103 (2013)

- Gleason, B., Richardson, K., Sissen, L., Smith, C.: Refractive index and thermo-optic coefficients of Ge–As–Se chalcogenide glasses. *Int. J. Appl. Glass Sci.* **7**(3), 374–383 (2016)
- Hu, J., Menyuk, C.R., Wei, C., Shaw, L.B., Sanghera, J.S., Aggarwal, I.D.: Highly efficient cascaded amplification using Pr³⁺-doped mid-infrared chalcogenide fiber amplifiers. *Opt. Lett.* **40**(16), 3687–3690 (2015)
- Jin, Y., Song, B., Jia, Z., Zhang, Y., Lin, C., Wang, X., Dai, S.: Improvement of Swanepoel method for deriving the thickness and the optical properties of chalcogenide thin films. *Opt. Express* **25**(1), 440–451 (2017)
- Laniel, J.M., Menard, J., Turcotte, K., Villeneuve, A., Vallee, R., Lopez, C., Richardson, K.A.: Refractive index measurements of planar chalcogenide thin film. *J. Non Cryst. Solids* **328**, 183–191 (2003)
- Maklad, M.S., Mohr, R.K., Howard, R.E., Macedo, P.B., Moynihan, C.T.: Multiphonon absorption in As₂S₃–As₂Se₃ glasses. *Solid State Commun.* **15**, 855–858 (1974)
- Marquez, E., Gonzalez-Leal, J.M., Prieto-Alcon, R., Vlcek, M., Stronski, A., Wagner, T., Minkov, D.: Optical characterization of thermally evaporated thin films of As₄₀S₄₀Se₂₀ chalcogenide glass by reflectance measurements. *Appl. Phys.* **67**, 371–378 (1998)
- Orava, J., Kohoutek, T., Wagner, T., Cerna, Z., Vlcek, M., Benes, L., Frumarova, B., Frumar, M.: Optical and structural properties of Ge–Se bulk glasses and Ag–Ge–Se thin films. *J. Non Cryst. Solids* **355**, 1951–1954 (2009)
- Petersen, C.R., Möller, U., Kubat, I., Zhou, B., Dupont, S., Ramsay, J., Benson, T., Sujecki, S., Abdel-Moneim, N., Tang, Z., Furniss, D., Seddon, A., Bang, O.: Mid-infrared supercontinuum covering the 1.4–13.3 μm molecular fingerprint region using ultra-high NA chalcogenide step-index fibre. *Nat. Photonics* **8**(11), 830–834 (2014)
- Poelman, D., Smet, P.: Methods for the determination of the optical constants of thin films from single transmission measurements: a critical review. *J. Phys. D Appl. Phys.* **36**, 1850–1857 (2003)
- Qiao, H., Anheier, N., Musgraves, J., Richardson, K., Hewak, D.: Measurement of chalcogenide glass optical dispersion using a mid-infrared prism coupler. *Proc. SPIE* **8016**(80160F), 1–10 (2011)
- Sanghera, J.S., Aggarwal, I.D.: Active and passive chalcogenide glass optical fibers for IR applications: a review. *J. Non Cryst. Solids* **256–257**, 6–16 (1999)
- Sanghera, J.S., Shaw, L.B., Aggarwal, I.D.: Chalcogenide glass-fiber-based mid-IR sources and applications. *J. Sel. Top. Quantum Electron.* **15**(1), 114–119 (2009)
- Schott Glass Inc.: Schott Infrared Chalcogenide Glass—IRG26 (2013)
- Seddon, A.B.: Chalcogenide glasses: a review of their preparation, properties and applications. *J. Non Cryst. Solids* **184**, 44–50 (1995)
- Seddon, A.B., Pan, W.J., Furniss, D., Miller, C.A., Rowe, H., Zhang, D.M., McBrearty, E.M., Zhang, Y., Loni, A., Sewell, P., Benson, T.M.: Fine embossing of chalcogenide glasses—a new fabrication route for photonic integrated circuits. *J. Non Cryst. Solids* **352**(23–25), 2515–2520 (2006)
- Seddon, A.B., Abdel-Moneim, N.S., Zhang, L., Pan, W.J., Furniss, D., Mellor, C.J., Kohoutek, T., Orava, J., Wagner, T., Benson, T.M.: Mid-infrared integrated optics: versatile hot embossing of mid-infrared glasses for on-chip planar waveguides for molecular sensing. *Opt. Eng.* **53**(7), 071824-1–071824-9 (2014)
- Swanepoel, R.: Determination of the thickness and optical constants of amorphous silicon. *J. Phys. E: Sci. Instrum.* **16**, 1214–1222 (1983)
- Swanepoel, R.: Determining refractive index and thickness of thin films from wavelength measurements only. *Opt. Soc. Am.* **2**, 1339–1343 (1985)
- Tang, Z., Furniss, D., Fay, M., Sakr, H., Sojka, L., Neate, N., Weston, N., Sujecki, S., Benson, T.M., Seddon, A.B.: Mid-infrared photoluminescence in small-core fiber of praseodymium-ion doped selenide-based chalcogenide glass. *Opt. Mater. Express* **5**(4), 870–886 (2015)
- Wang, Y., Qi, S., Yang, Z., Wang, R., Yang, A., Lucas, P.: Composition dependences of refractive index and thermo-optic coefficient in Ge–As–Se chalcogenide glasses. *J. Non Cryst. Solids* **459**, 88–93 (2017)
- Zakery, A., Elliott, S.: Optical properties and applications of chalcogenide glasses: a review. *J. Non Cryst. Solids* **330**(1), 1–12 (2003)